Current Research in Structural Biology 11 (2026) 100189

Contents lists available at ScienceDirect

Current Research in Structural Biology

journal homepage: www.journals.elsevier.com/current-research-in-structural-biology

Research Article

Crystal structure of 3-hydroxypropionyl-CoA synthetase (ADP-forming) from *Nitrosopumilus maritimus*

Jerome Johnson [a], Bilge Tosun [a], Merve Yilmaz [a,b,c], Bradley B. Tolar [d,e], Yasuo Yoshikuni [f], Christopher A. Francis [d], Tzanko Doukov [g], Shun Yokoi [g,h], Soichi Wakatsuki [g,i,*], Hasan DeMirci [a,j,**]

[a] MBGE Department, Koç University, Istanbul, 34450, Turkey
[b] Structural Biology, Max Delbrück Center for Molecular Medicine, Berlin, Germany
[c] Institute of Chemistry and Biochemistry, Freie Universität Berlin, Berlin, Germany
[d] Department of Earth System Science, Stanford University, Stanford, CA, 94305, USA
[e] Department of Biology and Marine Biology, University of North Carolina Wilmington, Wilmington, NC, 28403, USA
[f] The US DOE Joint Genome Institute, Lawrence Berkeley National Laboratory, Berkeley, CA, 94720, USA
[g] Department of Structural Biology, Stanford University, Stanford, CA, 94305, USA
[h] International Institute for Integrative Sleep Medicine (WPI-IIIS), Tsukuba Institute for Advanced Research (TIAR), University of Tsukuba, Tsukuba, 305-0005, Japan
[i] Biosciences Division, SLAC National Accelerator Laboratory, Menlo Park, CA, 94025, USA
[j] Stanford PULSE Institute, SLAC, Menlo Park, CA, 94110, USA

ARTICLE INFO

Handling Editor: Dr. N Strynadka

Keywords:
Thaumarchaeotal 3HP/4HB cycle
Carbon fixation
Acyl-CoA synthetase
Protein X-ray crystallography

ABSTRACT

The 3-hydroxypropionate/4-hydroxybutyrate (3HP/4HB) cycle in thaumarchaeota contributes significantly to global organic carbon fixation as the most energetically efficient aerobic carbon fixation pathway. The thaumarchaeal 3-Hydroxypropionyl-CoA Synthetase (ADP-forming; Nmar_1309) is crucial to this efficiency, utilizing ATP to ADP catalysis. This first reported structure of Nmar_1309 reveals a homodimer with a unique domain organization and a distinct linker between subdomains 4 and 1. This structure includes the bound substrates 3HP, non-hydrolyzable ATP (ADPNP), and a phosphate which suggest an intermediate state mimicking the non-covalent interaction between 3-hydroxypropionyl-phosphate and the active site histidine prior to reaction with Coenzyme-A. Conformational differences were observed between the two chains of the homodimer, likely influenced by the binding of a single ADPNP molecule in one chain. Phylogenetic analysis suggests that while 4HB synthetases may have evolved earlier in the evolutionary timeline, 3HP synthetases in Thaumarchaeota may have occurred after the Great Oxygenation Event. These structural data provide further characterization of the 3HP/4HB cycle and, in conjunction with the structure of 4-hydroxybutyryl-CoA synthetase, Nmar_0206, provide baseline structures of the key ADP-forming Acyl-CoA synthetases within this pathway.

1. Introduction

The looming climate crisis has been accelerated with reports that between January 2023 and January 2024 the average surface temperature of the earth surpassed a critical threshold of 1.5°C above those seen a century ago (World Meteorological Organization, 2024). To combat increased greenhouse gases, the study of biological processes and enzymes uniquely suited to fix atmospheric carbon has become an international endeavor. One such system, the Thaumarchaeotal 3-hydroxypropionate/4-hydroxybutyrate cycle (3HP/4HB cycle), has been identified as the most efficient aerobic carbon fixation cycle currently described (Könneke et al., 2014). This cycle, which fixes two carbon dioxide molecules in the form of bicarbonate and leads to the formation of the major end products acetyl- and succinyl-CoA, passes through the important intermediates 3-hydroxypropionate (3HP) and 4-hydroxybutyrate (4HB) (see Fig. 1). Significant variations have been found between Thaumarchaeotal and Crenarchaeotal enzymes used in the cycle which result in oxygen tolerance, bifunctionality and reduced energetic cost per metabolite formed in Thaumarchaeota (Könneke et al., 2014; Johnson et al., 2024; Destan et al., 2021; DeMirci et al., 2020; Berg et al., 2007). These enzymes result in the Thaumarchaeal

* Corresponding author. Department of Structural Biology, Stanford University, Stanford, CA, 94305, USA.
** Corresponding author. MBGE Department, Koç University, Istanbul, 34450, Turkey.
E-mail addresses: soichi.wakatsuki@stanford.edu (S. Wakatsuki), hdemirci@ku.edu.tr (H. DeMirci).

https://doi.org/10.1016/j.crstbi.2026.100189
Received 11 November 2025; Received in revised form 27 January 2026; Accepted 10 March 2026
Available online 17 March 2026

Abbreviations

3HP	3-hydroxypropionate
4HB	4-hydroxybutyrate
ACD	(ADP-forming) Acyl-CoA Synthetase
AC-S	Acetyl-CoA Synthetase
ADPNP	non-hydrolyzable ATP
ALS	Advanced Light Source
BL	Beamline
IPTG	Isopropyl-β-d-thiogalactopyranoside
LB	Luria Broth
MSA	Multiple Sequence Alignment
Ni-NTA	Nickel Nitrilotriacetic acid
PDB	Protein Database
SCS	Succinyl-CoA synthetase
TLS	Translation, Libration, and Screw

3HP/4HB cycle being the most energetically efficient, aerobic carbon fixation pathway. Structural characterization of these enzymes will inform engineering efforts to develop improvements on natural sequestration methods.

Within the oligotrophic open oceans, Thaumarchaeota may fix as much as 1% of all the biologically fixed carbon (Ingalls et al., 2006). The (ADP-forming) 3-hydroxypropionyl-CoA synthetase (Nmar_1309, from the representative archaeon *Nitrosopumilus maritimus*) is a critical enzyme in their success as alternatives to the cycle utilize a less energy efficient, AMP-forming version of the enzyme. Nmar_1309 is a member of the (ADP-forming) Acyl-CoA Synthetase superfamily (ACD) of enzymes, each member of which catalyzes the formation of an acyl-CoA and ADP using ATP, CoA and an acyl containing compound as substrate (Könneke et al., 2014; Sánchez et al., 2000). Nmar_1309 and Nmar_0206 (4-hydroxybutyryl-CoA synthetase) are two of a number of ACDs identified within the *N. maritimus* genome. Although capable of catalyzing multiple substrates, their low catalytic efficiency relative to 3HP supported the identification of Nmar_1309 as a 3-hydroxypropionyl-CoA synthetase.

Succinyl-CoA synthetase (SCS) may be seen as a model for the ACD superfamily, as characterization of the ACD reaction mechanism and structural characteristics for ACDs were first identified in the SCS

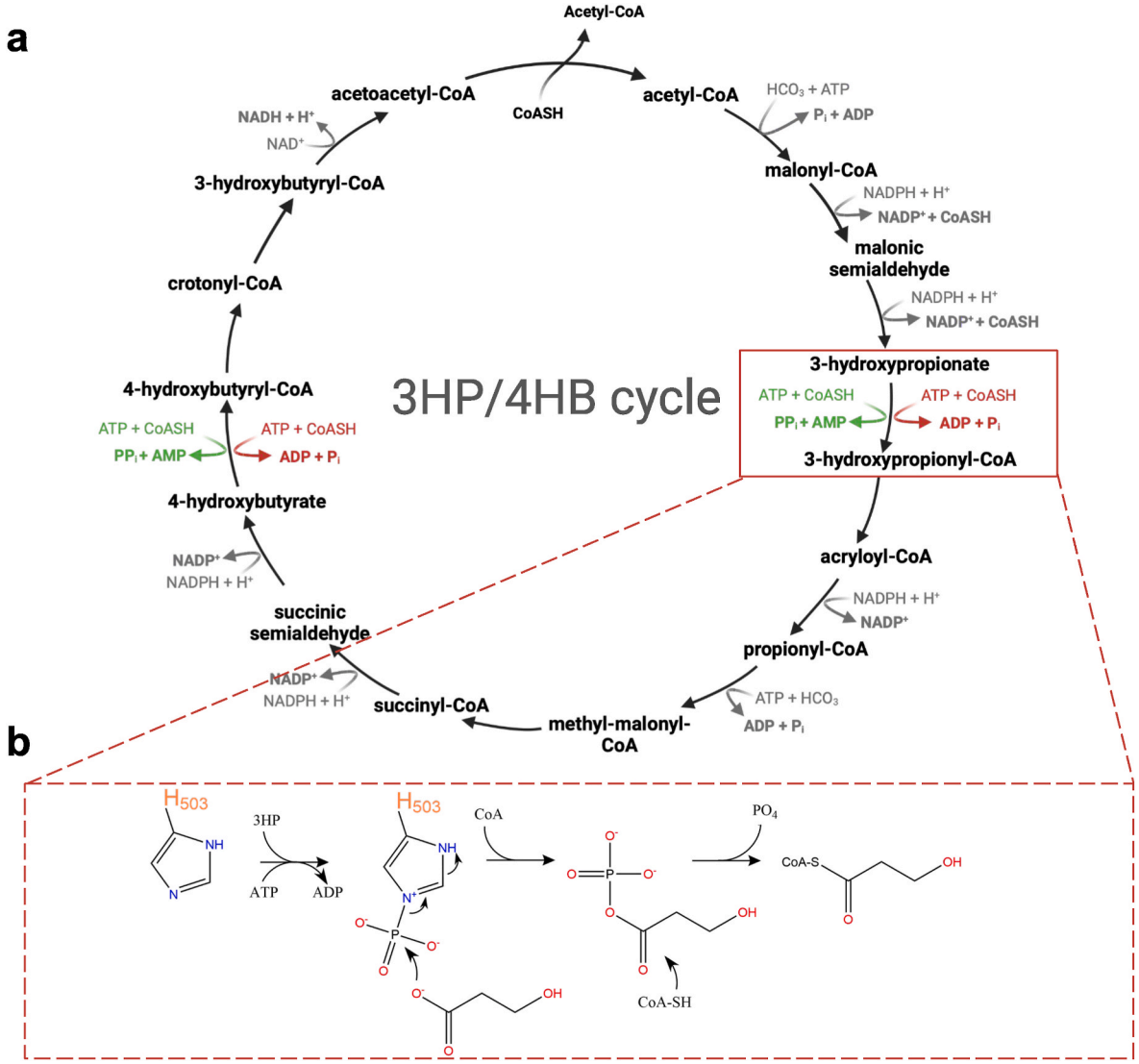

Fig. 1. The reactions involved in the HP/HB cycle for crenarchaeal and thaumarchaeal variants.
a The steps influencing the energy efficiency of the Thaumarchaeal 3HP/4HB cycle, specifically for *N. maritimus*, are highlighted in red while those for the crenarchaeotal variant are indicated in green. **b** Simplified reaction mechanism of Nmar_1309.

enzyme (Wolodko et al., 1994). ACD structures consist of CoA-binding, ligase and ATP-binding domains which are further distinguished into CoA-binding subdomains 1 and 2; ATP-binding subdomains 3 and 4; and CoA-ligase subdomain 5. In short, the reaction mechanism involves the dephosphorylation of the gamma phosphate of a bound ATP molecule resulting in the phosphate covalently bonded and passed to 1 or 2 histidine residues (Bräsen et al., 2008). This was proposed as members of the super family contain ATP-binding sites at varying distances from the active site. Structures with a relatively larger distance between the ATP-binding and active site, such as 31.5 Å within the larger 4-hydroxypropionyl-CoA synthetase compared to ~20 Å within the smaller SCS, require an additional histidine within the ATP-binding site to support catalysis. Regardless, due to the distances between the ATP binding site and the active site, a 'swinging-loop' containing the primary histidine bridges the distance between the two sites. After phosphorylation within the ATP binding site, this 'swinging-loop' returns to the active site where a nucleophilic attack by the acyl-group of the substrate molecule occurs. The histidine imidazole acts as the leaving group, resulting in an acyl-phosphate from which CoA may perform a nucleophilic attack with phosphate acting as a leaving group during the formation of the product Acyl-CoA (see Fig. 1) (Fraser et al., 1999).

This requirement to bridge large distances with flexible loops is a consequence of the remarkable structural diversity within the ACDs, which often arises from subdomain shuffling. This shuffling results not only in changes to the order of the protein primary structure (amino acid sequence) but also in oligomerization state, linkage and surface interaction variations (Johnson et al., 2024). The subdomain organization of ACD superfamily proteins can be described following nomenclature standardized by SCS: [α(1,2)/β(3,4,5)] for SCS (Fraser et al., 1999), [α(1,2,5)/β(3,4)] for Acetyl-CoA synthetase (pdb: 4XYM) (Weiβe et al., 2016), (World Meteorological Organization, 2024; Könneke et al., 2014; DeMirci et al., 2020; Johnson et al., 2024; Destan et al., 2021) for 4-hydroxybutyryl-CoA synthetase (Nmar_0206 from the same cycle) (Johnson et al., 2024) and (Johnson et al., 2024; Destan et al., 2021; World Meteorological Organization, 2024; Könneke et al., 2014; DeMirci et al., 2020) for Nmar_1309. From this organization, ACDs oligomerize into heterodimeric, homodimeric and heterotetrameric structures. These are found throughout all domains of life. To address how and why this structural diversity evolved, this study reveals the molecular architecture of Nmar_1309, providing the first structural snapshot of this unique domain arrangement within the ACD superfamily.

2. Materials and methods

2.1. Cloning

The *Nitrosopumilus maritimus* Nmar_1309 (3-hydroxypropionyl-CoA synthetase) gene sequence with an N-terminal hexahistidine tag was designed and codon-optimized using Genscript BioTech trademark software before synthesis for Ni-NTA affinity purification. Nmar_1309 was then cloned into the pET28a vector using *Nde*I and *Bam*HI endonuclease restriction sites, and transformed into *E. coli* strain BL21 (Rosetta-2). Transformed cells were selected for by growth in LB agar plates containing kanamycin (50 μg/ml) and chloramphenicol (50 μg/ml) at 37 °C.

2.2. Protein expression and purification

Expression of Nmar_1309 was performed using the BL21(Rosetta-2) *E. coli* transformed cells. Cultures were grown overnight in LB media and then diluted 1:100 into 2 L cultures. The cell cultures were grown to an optical density of 0.8 at 600 nm and then expressed overnight at 18 °C following induction with 0.4 mM IPTG. Cell pellet was then obtained following centrifugation at 3700×*g*, resuspended in a lysis buffer (pH 8.5 50 mM Tris, 300 mM NaCl, 5% v/v glycerol supplemented with 0.01% Triton X-100), and sonicated. Soluble protein was maintained at 4 °C, purified using Ni-NTA affinity resin (GE Healthcare) and concentrated to 10 mg/ml using 50 kDa Amicon concentrators. The column was equilibrated with pH 8.5 HisA (containing 300 mM NaCl and 20 mM Tris). A column wash was performed using pH 8.5 HisA and the proteins were eluted with pH 8.5 HisB (containing 500 mM imidazole, 300 mM NaCl, 50 mM Tris). Following purification, the His_6-tag was removed overnight at 4 °C by thrombin digestion in the presence of 5 mM β-mercaptoethanol. Reverse Ni-NTA was then performed to remove the thrombin-cleaved His_6-tag. Nmar_1309 purity was confirmed through SDS-PAGE. Following purification, 20 mL of 50% glycerol was added to 30 mL of the enzyme elutant for long-term storage.

2.3. Crystallization

Crystallization screens were performed using 72-well Terasaki microbatch plates. 0.83 μL of purified Nmar_1309 were pipetted into the bottom of the sitting drop and mixed with an additional 0.83 μL of ~3500 commercially available sparse-matrix crystallization screening conditions (Atalay et al., 2023), followed by a 16.6 μL application of Paraffin oil. Plates were stored in styrofoam containers at room temperature and crystals of Nmar_1309 were obtained 1-2 weeks after initial crystallization screenings. Protein crystals were obtained in a solution of 2.5 μL of 200 mM Magnesium chloride hexahydrate, 100 mM Tris pH 8.5, 7% (v/v) PEG 6000 with 2.5 μL of the enzyme solution, covered with ~50 μL of Paraffin oil.

2.4. Data collection and processing

Protein crystals of Nmar_1309 in mother liquor supplemented with 20% v/v glycerol for cryoprotection were prepared for crystallography by flash freezing in liquid nitrogen. The data was collected at the Advanced Light Source Beamline 5.0.2 at the Lawrence Berkeley National Laboratory, Berkeley, California, USA. The detector distance for the enzyme structure was set at 400 mm with an exposure time of 0.2 s per frame, with the X-ray energy set to 12.398 keV. The diffraction data were collected to 2.8 Å resolution at 100 K. The crystal belongs to the space group $P2_12_12_1$ with unit cell dimensions a = 81.88 Å, b = 127.59 Å, c = 137.76 Å, α = 90, β = 90, and γ = 90 [see Table 1]. The diffraction data were processed with the XDS package (Kabsch, 2010) for indexing and scaled by using XSCALE. STARANISO was used to further improve the data (Tickle et al., 2016).

2.5. Structure determination and refinement

An AlphaFold2 generated model was used as a search model for automated molecular replacement using *PHASER* within the Phenix software suite (Adams et al., 2010). This was followed by simulated-annealing, individual coordinate and TLS parameters refinement. Coot (version 0.9.8.1) was then used to confirm residue and water positions, and addition of residues missing in the electron density map (Emsley and Cowtan, 2004). Further refinement was performed to 2.8 Å resolution within Coot and Phenix while maintaining positions with strong difference densities and Ramachandran statistics for the structure were optimized to 97.9/1.7/0.4% (most favored/additionally allowed/disallowed) [see Table 1 for full refinement statistics]. The final R-work and R-free were 0.21 and 0.25, respectively. Structural figures were generated using PyMOL (version 2.5.2; Schrödinger (2021). Coordinates of the final refined model were submitted to the Protein Data Bank (PDB)(RCSB.org) (Berman et al., 2000) and assigned the identifier 9Y43.

2.6. Phylogenetic and residue conservation analysis

NCBI Protein BLAST (blastp) was used to search for homologous sequences using Nmar_1309, Nmar_0206, acetyl-CoA synthetase (ADP-

Table 1
Data collection and refinement statistics for Nmar_1309.

PDB ID	**9Y43**
Diffraction cut-off criterion	**Local <I/sd(I)> = 1.20**
Semi-axis d-spacings (Ang.) and corresponding principal axes of the ellipsoid fitted to the diffraction cut-off surface:	
Diffraction limit #1: 2.934 (1.0000, 0.0000, 0.0000) a*	
Diffraction limit #2: 2.777 (0.0000, 1.0000, 0.0000) b*	
Diffraction limit #3: 3.450 (0.0000, 0.0000, 1.0000) c*	
Data collection	
X-ray source	*ALS BL5.0.2*
Wavelength (Å)	*1.000*
Space group	P $2_12_12_1$
Cell dimensions	
a, b, c (Å)	81.88 127.59 137.76
α, β, γ (°)	90.00 90.00 90.00
Resolution (Å)	48.7-2.8 (3.0-2.8)
CC (½)	0.99 (0.43)
*CC**	0.99 (0.78)
I/σI	9.3 (1.4)
Completeness (spherical)	*72.3 (17.1)*
Completeness (ellipsoidal)	92.6 (61.4)
Redundancy	13.1 (13.3)
Refinement	
Resolution (Å)	48.7-2.8 (2.9 -2.8)
No. reflections	26 591 (332)
R_{work}/R_{free}	0.21/0.25 (0.35/0. 40)
No. atoms	
Protein	10599
Ligand/Ion/Water	200
B-factors (Å^2)	
Protein	53.3
Ligand/Ion/Water	48.9
R.m.s deviations	
Bond lengths (Å)	0.037
Bond angles (°)	2.32
Ramachandran plot	
Favored (%)	97.9
Allowed (%)	1.7
Disallowed (%)	0.4

[1]Values in parentheses are for the highest-resolution shell. Data were anisotropically truncated using the Staraniso server; completeness statistics are reported with respect to the elliptical resolution limits.

forming) from *Candidatus* Korarchaeum cryptofilum, and Human Succinyl-CoA Synthetase (ADP-forming) as separate query templates (NCBI WP_012215692.1, WP_012214589.1, WP_012308855.1, and NP_003840.2, respectively) (Altschul et al., 1990, 1997). 45 sequences were selected based on species identifiers and used to construct a multiple sequence alignment (MSA) in MEGA (v11.0.13) with the default settings for CLUSTALW program (v2.1) (Tamura et al., 2011, 2021). This MSA was used to generate an amino acid-based phylogenetic tree of ACDs by the neighbor-joining method, using default settings within MEGA. The phylogenetic tree was then visualized with the iTOL: Interactive Tree of Life webserver (Letunic and Bork, 2021). The Consurf web server was used to estimate evolutionary conservation at each amino acid position with default parameters and automatic homolog selection (Yariv et al., 2023). Interprosurf was used for interface area and hydrophobicity analysis (Negi et al., 2007).

2.7. Accession numbers

PDB: 9Y43.

3. Results and discussion

3.1. Overall homodimeric Nmar_1309 structure

The 3-hydroxypropionyl-CoA synthetase Nmar_1309 is a homodimer consisting of CoA- and ATP-binding domains. These domains can be further subdivided into two CoA-binding subdomains (1&2), two ATP-grasping subdomains (3&4), and a CoA-ligase subdomain (5). The sequences and overall structure are very similar to previously determined structures for other ACDs except for the characteristic domain shuffling resulting in a unique linker between the 4th and 1st subdomains and an overall subdomain sequence of [3-4-1-2-5](see Fig. 2). Subdomain 1 adopts a canonical Rossmann fold positioned to bind the adenyl moiety of CoA, consistent with homologous structures. The composite active site is formed at the dimer interface between subdomains 2 and 5 of opposing monomers. Here, 3HP is positioned to react with the pantetheine thiol of CoA to form the 3HP-CoA thioester. Subdomain 2 also contains the catalytically important 'swinging-loop' (T493-S510) which bridges the ~38 Å distance between the ATP-grasping and CoA-binding sites. In the crystal structure, the loop is captured with His503 at its tip coordinating a bound phosphate.

Subdomains 3 and 4 collectively constitute the ATP-grasp domain, with subdomain 3 inserted within the sequence of subdomain 4. The homodimer displays significant conformational asymmetry. Chain An undergoes a ~16° domain closure to sequester the bound ADPNP, utilizing residues Pro36 and Lys116 as hinge points. A 19-residue interdomain linker (Asn231–Asp248) extends from the C-terminus of subdomain 3, covalently tethering the ATP-grasp and CoA-binding domains. This covalent linkage underpins the homodimeric architecture of Nmar_1309. This organization contrasts with the topologically distinct linker in Nmar_0206 and the complete absence of linkers in homologous heterotetrameric or heterodimeric structures (See Fig. 2).

3.2. Domain shuffling: comparison with homologs Nmar_0206, acetyl-CoA synthetase and succinyl-CoA synthetase reveals structural differences

We have compared Nmar_1309 with its homologs Nmar_0206 (pdb:8WZU), Acetyl-CoA Synthetase (ADP-forming) from *Ca.* Korarchaeum cryptofilum (hereafter referred to as AC-S; pdb:4XYM) and Human Succinyl-CoA Synthetase (ADP-forming) (SCS; pdb:6G4Q) which share 36%, 38% and 22% sequence identity respectively. While Nmar_1309 has a domain organization [3-4-1-2-5], Nmar_0206 is organized [1-2-5-3-4], AC-S [α(1,2,5)/β(3,4)] and SCS [α(1,2)/β(3,4,5)] with α and β referring to separate chains for the ATP- and CoA binding domains (see MSA in Supplementary Fig. 1). This domain shuffling between Nmar_1309 and its homologs is a common characteristic of the ACD superfamily. The observed domain shuffling suggests structural differences in the 3HP/4HB enzymes compared with their homologs and might give insights into their environmental variation in their evolutionary history. Previous studies have shown that other enzymes demonstrating shifts in domain organization present differing surface regions for regulation, change reaction chemistry, or even catalyze completely different reactions (Bräsen et al., 2008; Saier and Reizer, 1990; Oliynyk et al., 1996).

The active site of Nmar_1309 lies at the interface between subdomains 1, 2, and 5 (Fig. 2). Subdomains 1 and 2 seem largely paired in homologous structures to maintain the active site and, as their relative N- and C-termini lie behind these subdomains (with respect to the active site), would therefore require a long linker to wrap around the structure to bring a directly bound subdomain 5 to that same active site for interaction (Supplementary Fig. 2: Supplementary Fig. 3). Citrate lyases seem to uniquely contain a large linker between these subdomains and display the monomeric form [3-4-5-1-2-CS] (CS being the citrate synthase homology subdomains unique to these structures). This unique organization supports the distinct catalytic role of citrate lyase. While ACDs like Nmar_1309 function solely to form and release acyl-CoA thioesters, citrate lyase utilizes the conserved synthetase mechanism to drive the cleavage of citrate—effectively the reverse of the citrate synthase reaction. The enzyme generates a transient citryl-CoA intermediate using the conserved ATP-dependent mechanism; however, instead of releasing this intermediate, the fused C-terminal CSH domain immediately catalyzes its cleavage into acetyl-CoA and oxaloacetate. To

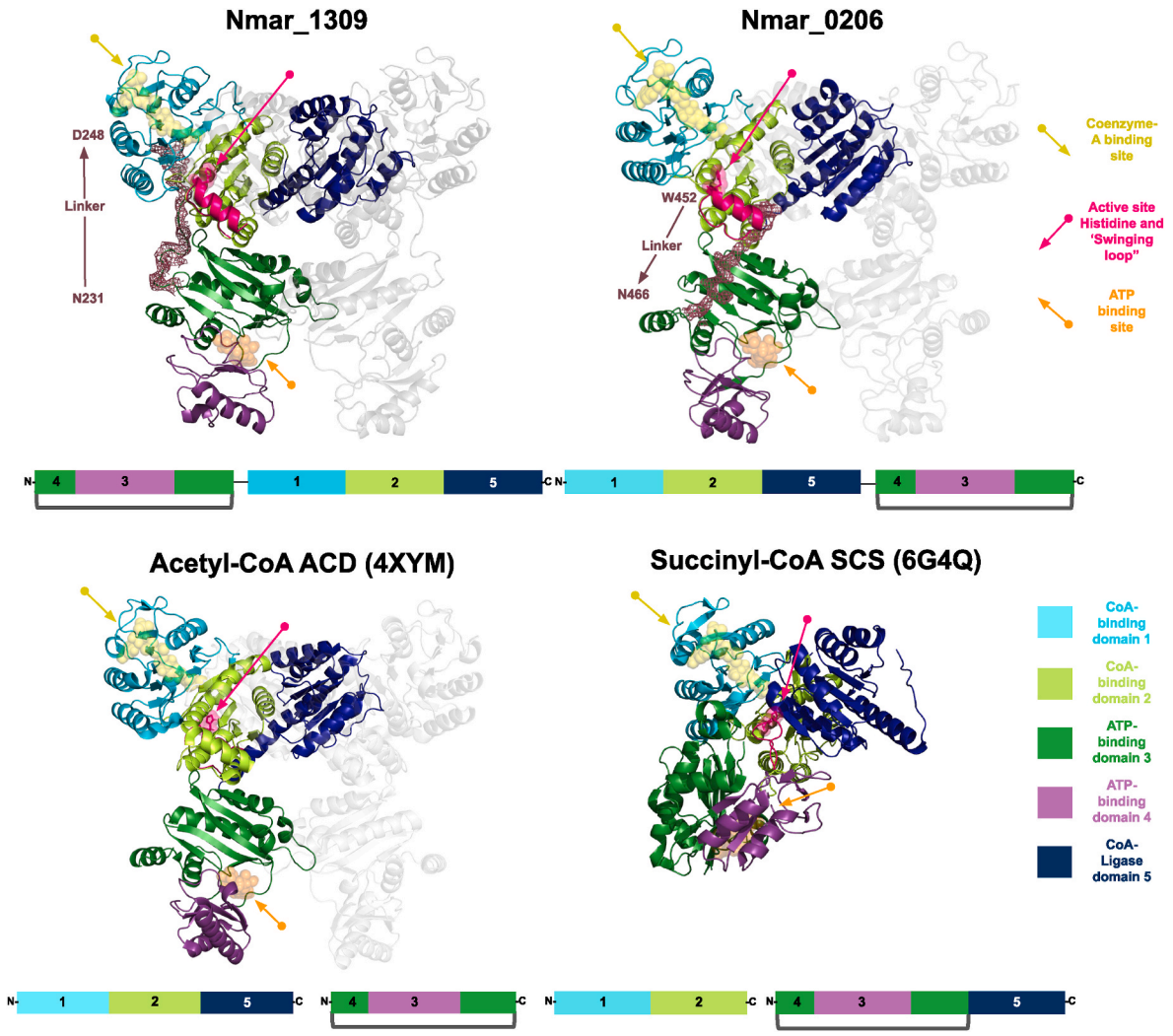

Fig. 2. Domain organization comparison of Nmar_1309 protein with its homologs Nmar_0206, *Ca.* Korarchaeum cryptofilum acetyl-CoA synthetase and Human succinyl-CoA synthetase.

Domain organization of domains 1 (teal), 2 (limon-green), 3-4 (forest-green and purple), and 5 (dark blue) are shown between homologs. Nmar_1309 and _0206 linker directionality is indicated by the arrow, along with starting and ending residues, and their respective densities are highlighted in red. Coenzyme-A (yellow) and ATP (orange) binding sites are also indicated by arrows, and their locations are shown by transparent blobs. The active site histidine and associated 'swinging-loop' is shown in pink, with the active site histidine pointed towards the active site.

our knowledge no structure has been published to pdb with a resolved linker, so the exact orientation of these linkers are unknown. With citrate lyases as an exception, the structural limitations of directly linking subdomains 1, 2 and 5 in such a way that forms an active site seems evolutionarily constrained.

In Nmar_1309, a solvent-exposed linker region further contributes to structural integrity through interactions with subdomains 4 (N231, K232, K234, K235, N237, and S238), 2 (S240 and S245), and 1 (D248) (Supplementary Fig. 4). These interactions may enhance the stability and dynamic communication between subdomains, potentially influencing its functional properties.

To further inspect the role of linkers between the CoA-binding and ATP-binding domains of Nmar_1309, we compared interdomain interfaces between homologs with different oligomeric forms. Nonpolar interactions are vital for the formation of functional dimeric enzymes (Levy et al., 2013). While this was true for the four structures studied, variation in the hydrophobicity of the interface may speak to variability in the overall strength of the interfaces of these oligomers and, by extension, energetic environmental constraints. With regards to interfaces between the identical functional subunits (i.e., between chain A and B of Nmar_1309, and chains A/B and chains C/D of AC-S), relative levels of polar interactions between the four oligomeric forms were Nmar_1309 (32%) > SCS (31%) > AC-S (24%) > Nmar_0206 (23%) (see Fig. 3), with nonpolar interactions being the inverse. This may be explained in part by the relative surface area size of the Nmar vs AC-S structures, with the SCS structure being an outlier as the general curvature of the interface may support greater hydrophilicity.

The interfaces between CoA- and ATP-binding domains, however, tell a different story. Firstly, both Nmar structures have smaller interfaces than AC-S (1362 Å^2 and 1054 Å^2 vs 1546 Å^2). Secondly, the AC-S structure has a much higher interface hydrophilicity between the CoA- and ATP-binding domains when compared to the interface between the chains (24% to 34%). While this trend is true for the Nmar interfaces (Nmar_1309: 32% to 34% and Nmar_0206: 23% to 29%), the relative increase in AC-S is much greater (10% increase vs 6% and 2%). As these interface areas are much smaller, this potentially suggests the need for the increased hydrophilicity with the linker itself reducing that need by stabilizing the structure without these bonds as previously proposed (Johnson et al., 2024).

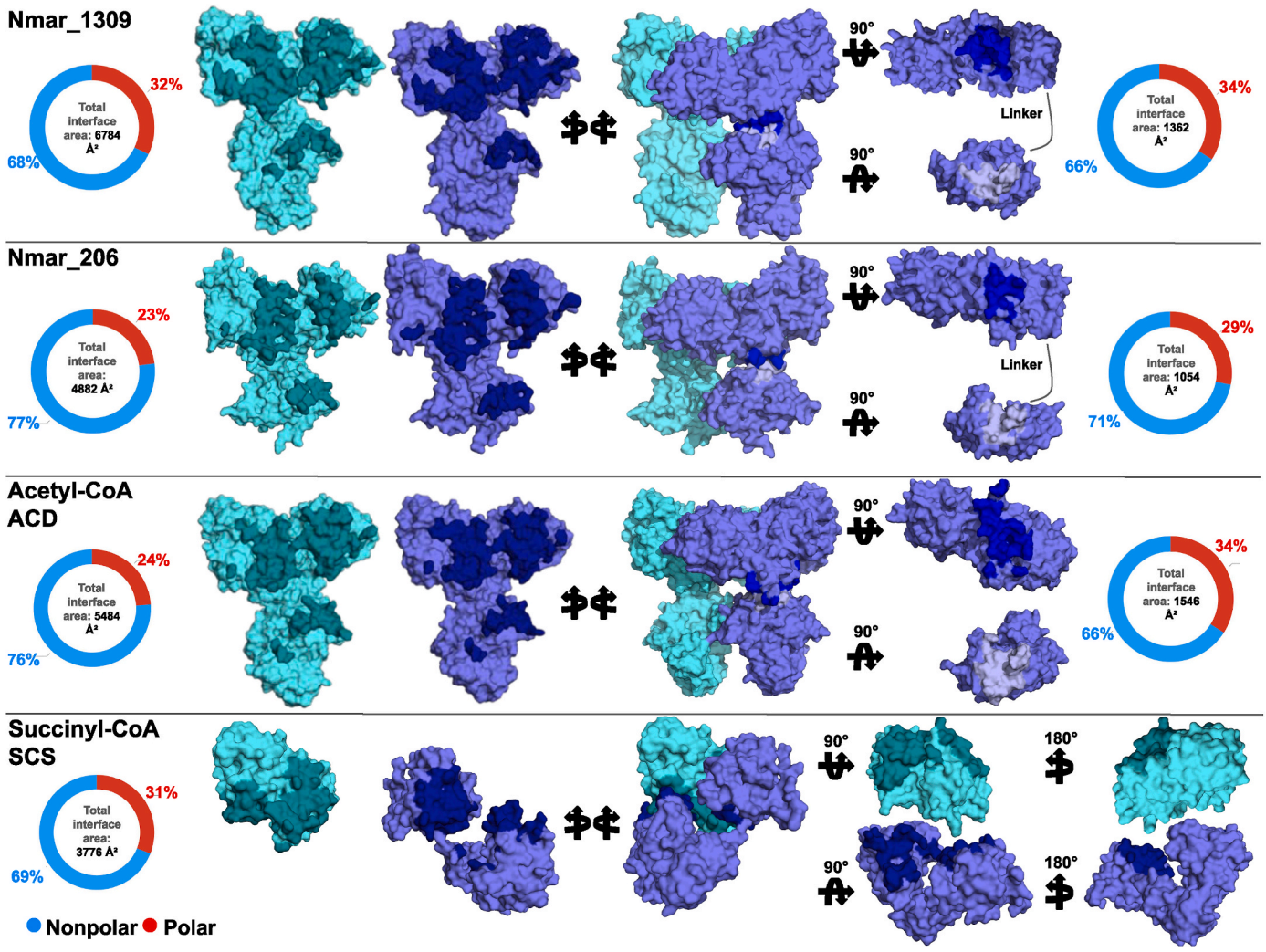

Fig. 3. Comparison of interface surfaces of Nmar_1309, Nmar_0206, AC-S, and SCS.
Chains A (teal) and B (slate) of Nmar_1309 and Nmar_0206 as well as the respective sites in AC-S and SCS are shown. Combined interface area between the Chains (left) as well as the ADP- and CoA-binding domains (right) are highlighted in differing shades. The pie charts show nonpolar (blue) and polar (red) surfaces.

3.3. Phylogenetics suggest the divergence of 3HP from 4HB synthetases occurred following the great oxygenation event

Phylogenetic analysis of homologous structures with different oligomerization states largely grouped into separate clades. There is a stark separation between citrate lyases and SCSs and other groups studied (Fig. 4). This may be linked partly to the ability for citrate lyases and SCSs to form functional CoA lyase active sites from single functional units. Within the further delineated AC-S, 4HB, and 3HP synthetase clades, it has previously been noted that bacteria occupy an intermediate position between AC-Ss and the other clades, suggesting horizontal gene transfer[3]. This is further supported by the findings that a high number of genes within thaumarchaeal genomes appear to originate in Bacteria (instead of Archaea) (Ren et al., 2019).

A previously described evolutionary timeline mapped thaumarchaeal divergence from crenarchaeota and euryarchaeota to the great oxygenation event (Ren et al., 2019). Interestingly, a few crenarchaeal 4HB synthetase homologs analyzed here formed their own clade between Thaumarchaeotal 3HP and 4HB synthetases (Fig. 4). This includes the model organism *M. sedula* used to originally describe the 3HP/4HB cycle but which generally uses the less energetically efficient AMP-forming versions of these enzymes (Könneke et al., 2014; Berg et al., 2007). The fact that crenarchaeal homologs clustered between the two thaumarchaeal enzymes suggest that the divergence between the 3HP and 4HB enzymes in Thaumarchaeota may have happened following the oxygenation of the oceans (Ren et al., 2019). The close homology of Thermoproteota AC-S and thaumarchaeal 4HB synthetases may indicate that these evolved earlier in the evolutionary timeline.

3.4. Structural comparison of chain A and chain B of Nmar_1309 demonstrates conformation differences in the ATP-binding domain

The Nmar_1309 structure contains 3 ligands and 2 bound phosphate molecules functionally relevant to the reaction mechanism. Within each active site at the juncture of the CoA-binding and ligase-CoA subdomains, 3HP can be found stabilized by the presence of a phosphate at the head of two 'powerhelices' (Wolodko et al., 1994). Furthermore, a single ADPNP is bound in the ATP-binding domain of chain A but not chain B (see Fig. 5a–b). The well defined electron densities in this region display conformational differences essential for the binding and stabilization of ATP before dephosphorylation (see Fig. 5c–d; Fig. 6, Supplementary Fig. 5). When the monomers are aligned, a ~15.6° rotation of the ATP-binding domain of chain A can be seen closing towards the bound ADPNP (averaged across residues H69, R96 and K88 with M111 as a stable reference; see Fig. 5e and Supplementary Fig. 6). In contrast, Chain B, shows an electron density map without the ligand displaying a more open conformation rotated away from the binding site.

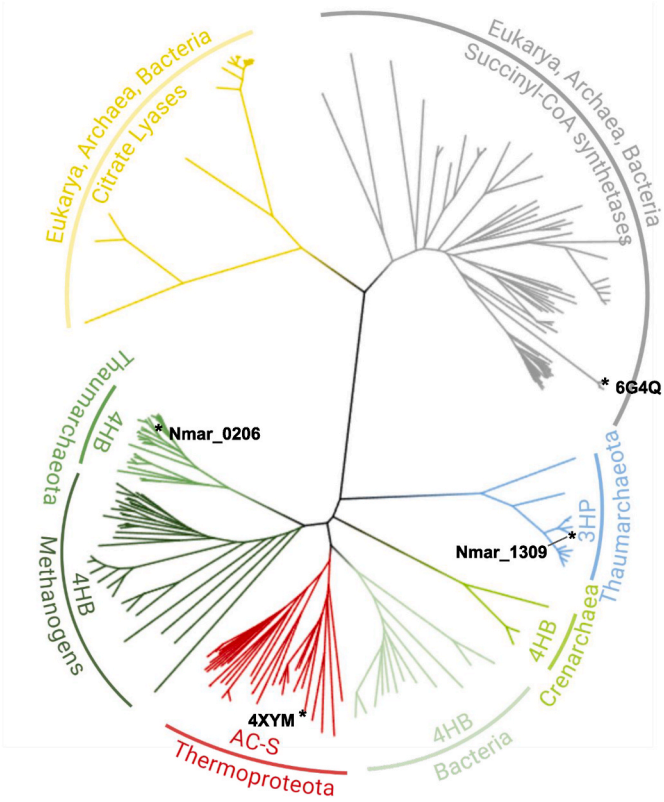

Fig. 4. Phylogenetic tree of Nmar_1309 and homologues
This tree highlights the strong divergence between enzymes with different oligomerization structures. Heterodimeric SCSs and homohexameric Citrate Lyase structures with the domain organization x-1-2-3-4-5 (x being unique to these enzymes) makeup a clade separate from heterotetrameric AC-Ss and homodimeric 3HP and 4HB synthetases. While citrate lyases and SCSs are present in Eukarya (not separated for simplicity), none of the other groups are found in Eukarya. Asterisks (*) indicate structures that were compared in Fig. 2 (i.e., Thaumarchaeota Nmar_0206 4HB and Nmar_1309 3HP, Thermoproteota Acetyl-CoA 4XYM AC-S, and Succinyl-CoA Synthetase SCS 6G4Q).

3.5. Observed binding modes of 3HP and phosphates in Nmar_1309 offer insight into reaction mechanisms

The crystal structure reveals two 3HP molecules, one bound at each active site to H503 and a phosphate molecule. Due to the low resolution of the model, two opposite-facing conformations of each 3HP were placed within the density and occupancy refined (See Supplementary Fig. 7). Our results show that the 3HP molecules favor the binding orientation seen in homologous proteins (i.e., carboxylate end oriented towards the phosphate refines to 70% occupancy in chain A and 74% in chain B; see Supplementary Fig. 8) and are suggested by the reaction mechanism itself (See Fig. 6) (Weiβe et al., 2016; Verschueren et al., 2019; Huang and Fraser, 2016). This major conformer was selected for the final refinement.

3.6. Reaction mechanism of Nmar_1309 and structural localization

The reaction mechanism for ACDs has been established by several previous studies (Wolodko et al., 1994; Bräsen et al., 2008; Fraser et al., 1999, 2002; Weiβe et al., 2016; Verschueren et al., 2019; Huang and Fraser, 2016; Joyce et al., 2000; Bailey et al., 1999; Fan et al., 2012). The presence of an additional histidine in the ATP-binding site supports the 2 histidine reaction mechanism (Bräsen et al., 2008). This is one of two mechanisms known for ACDs which have been described as distinguishing SCSs from other ACDs. SCS originally described a reaction mechanism involving a single histidine on the aforementioned swinging loop; subsequently ACDs were described as requiring an additional histidine in the ATP binding site due to slight difference in reaction chemistry (Wolodko et al., 1994; Bräsen et al., 2008). All residues involved have been inferred by sequence alignment and from their respective locations upon superposition.

The reaction begins with the binding and dephosphorylation of the gamma phosphate of ATP by H69 within the ATP binding pocket (Wolodko et al., 1994; Fraser et al., 1999, 2002; Joyce et al., 2000). The removed phosphate is initially covalently bound to H69 but is subsequently passed to H503 which, attached to the flexible 'swinging loop', swings into the reaction center between subdomains 1, 2 and 5 upon phosphorylation (Fraser et al., 1999; Weiβe et al., 2016; Huang and Fraser, 2016; Joyce et al., 2000). Stabilized by the positively charged dipole of the power helices and potential interactions with other neighboring residues (such as E462 and D602′), at this point, phospho-His503 is available for interaction with 3HP (Weiβe et al., 2016; Huang and Fraser, 2016). Incoming 3HP performs a nucleophilic attack on phosphoHis503, with the histidine imidazole acting as a leaving group. The formed acyl-phosphate is left susceptible to nucleophilic attack by CoA to peel off the 3HP, freeing phosphate and forming 3HP-CoA (Weiβe et al., 2016; Fan et al., 2012).

Although unphosphorylated, this structure of Nmar_1309 appears to be temporally located similar to a phosphorylated H503 in the CoA-binding active site interacting with 3HP just before the attack of 3HP on the phosphoHis503 (see Fig. 6, step 4). Both active sites show interactions predicted at that step between D602′, Phosphate, H503 and a bound water (with the exception of a single bond in chain A and the obvious lack of a covalent bond between phosphate and histidine; see Fig. 7). This being said, many interactions which can be seen were not reported in homologous structures including with N376, G558′, A557′, G412, T413, N555, D636′, V434 and additional waters. Most of these interactions are shared between the two active sites with exceptions in the single additional D602'; the additional interactions with 3HP, V434 and an intermediate water; and those of the additional water between 3HP, phosphate, N555 and D602'. While these interactions may just be a product of the bound phosphate instead of phosphohistidine at this reactive step, they may reflect similar interactions in the real reaction mechanism thus far unelucidated.

4. Conclusion

The efficiency of global carbon fixation is driven by diverse enzymatic pathways, with the thaumarchaeal 3HP/4HB cycle standing out for its energetic optimization. Our analysis of Nmar_1309 reveals key evolutionary and structural adaptations that underpin this cycle's success. The evolution of Nmar_1309 seems tied to the evolution of Thaumarchaeota, with its divergence from Nmar_0206 and other ACDs potentially a later development in evolutionary history. Domain shuffling is characteristic of ACDs and allows evolutionary flexibility in how these structures are organized resulting in a number of oligomeric types (see Fig. 2). Linkers between chains play an important role in stabilizing oligomerization and active site formation (see Fig. 3). A large physical distance between CoA-binding and CoA-lyase subdomains in a functional active site makes a direct linker between these a potential evolutionary barrier (see Fig. 4; see Supplementary Fig. 2). AC-S, 4HB, and 3HP synthetases seem to overcome this by oligomerizing. Citrate lyases, in contrast, do form this linker while SCSs form a heterodimer instead. Due to the evolutionary distance between these oligomerization states, this may suggest the evolutionary time required to transition to functional active sites in single asymmetric units.

Nmar_1309 and Nmar_0206 both have linkers between CoA-binding and ATP-binding domains but link on opposite ends of subdomain 3. It is worth noting that while many other archaea - particularly representatives from thermoproteota and crenarchaeota - contain both heterotetrameric and homodimeric forms of ACDs (4HB synthetases and AC-Ss), *Nitrospumilus* sp. do not. This could suggest the evolutionary

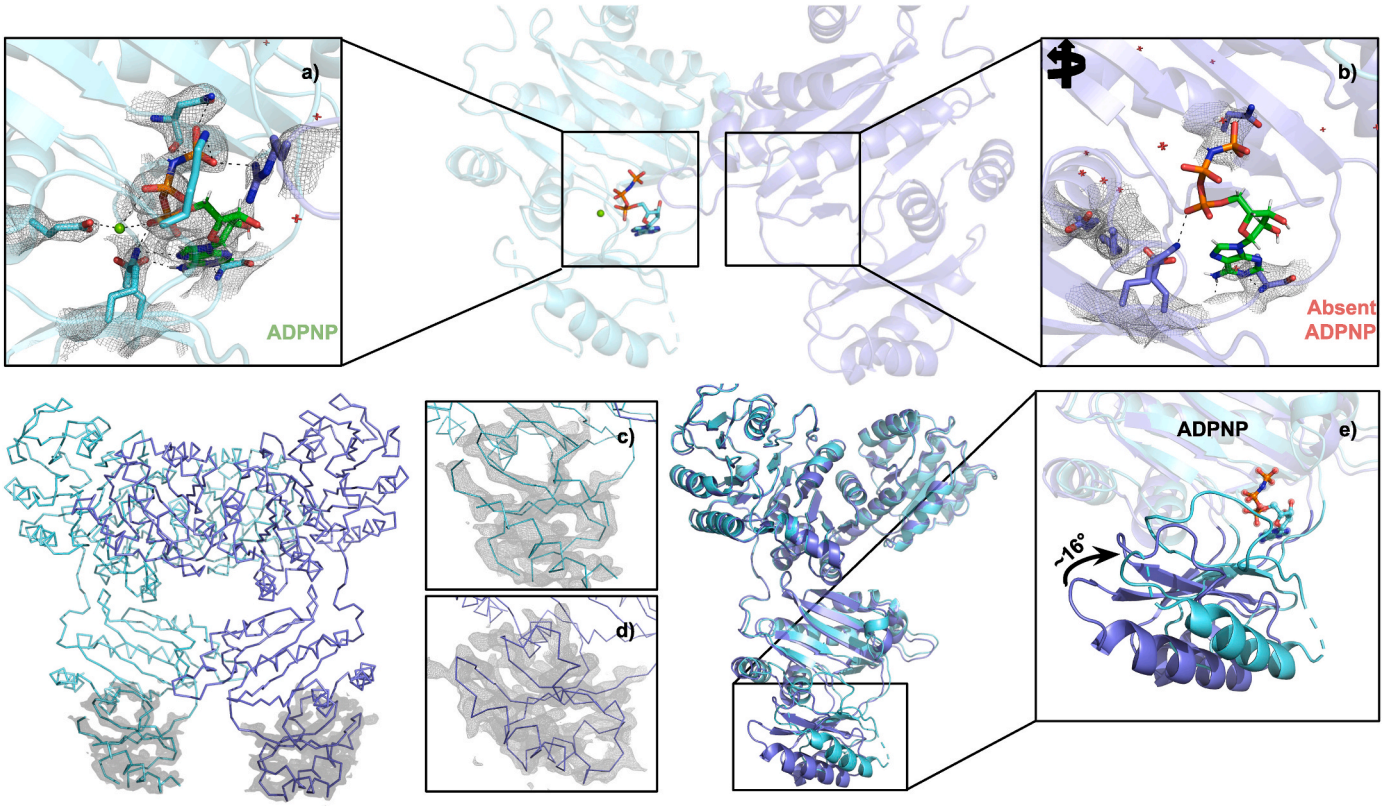

Fig. 5. Bound ligand densities and ATP-binding domain conformational shifts
Structural localization of ADPNP binding is shown here, along with electron densities from both chains of the dimer. **a** In Chain A, the ADPNP binding site and its electron density are shown, **b** while in Chain B, the electron density shows a lack of ADPNP (the one shown is placed at the relative location from a superposed chain A) at that same site. **c,d** The electron densities of the two chains' ATP-binding domains. **e** A structural alignment of Chain A and Chain B illustrates a ~16° rotation upon ADPNP bonding. The rotation was calculated by averaging the angles formed between the locally stable M111 residue and the shifted residues H69, R96, and K88. 2Fo-Fc electron density maps are shown with a contouring level of 1σ and carved to 2 Å.

benefit of a linker connecting CoA-binding and ATP-binding domains in oxygenic environments that formed during the evolution of Thaumarchaeota.

Many standard features of ACDs can be seen in the structure of Nmar_1309 including the catalytically important power helices, locally stabilized phosphate and bound 3HP at both active sites (see Fig. 7). Both active sites indicate very similar binding modes, suggesting a temporal stabilization near step 4 of the reaction mechanism while displaying many interactions not previously discussed (see Figs. 6 and 7). Whether these are a product of the free phosphate or reflect catalytically important interactions need further investigation.

This structural elucidation of Nmar_1309, particularly when combined with the structure of Nmar_0206, completes the characterization of key ADP-forming Acyl-CoA synthetases in the vital thaumarchaeal 3HP/4HB cycle. Considering the significant contribution of Thaumarchaeota to global carbon fixation, unraveling the structural and evolutionary intricacies of their metabolic enzymes—products of extensive adaptation and inherently sensitive to environmental shifts—is of profound importance. The detailed insights gained from such studies are fundamental not only for understanding natural biogeochemical processes but also for providing a robust blueprint for innovative bioengineering strategies to address pressing global challenges.

Data availability statement

The Nmar_1309 structure and associated files were deposited in the PDB under 9Y43. All other supporting data are available from the corresponding author upon reasonable request.

Permission to reproduce material from other sources

All content, figures, and tables presented in this manuscript are the original work of the authors. No material has been reproduced from other sources.

CrediT author statement

Hasan Demirci: Conceptualization, Methodology, Investigation, Writing- Reviewing and Editing. **Yasuo Yoshikuni**: Conceptualization, Writing- Reviewing and Editing. **Christopher A. Francis**: Conceptualization, Writing- Reviewing and Editing. ***Soichi Wakatsuki:*** Conceptualization, Methodology, Writing- Reviewing and Editing. **Jerome Johnson**: Methodology, Investigation, Formal analysis, Writing-Reviewing and Editing. **Bradley B. Tolar:** Investigation, Formal analysis, Writing- Reviewing and Editing. **Bilge Tosun:** Investigation, Writing- Reviewing and Editing. **Shun Yokoi:** Investigation, Writing-Reviewing and Editing. **Merve Yilmaz:** Investigation, Writing-Reviewing and Editing. **Tzanko Doukov:** Investigation, Writing-Reviewing and Editing.

Declaration of generative AI and AI-assisted technologies in the manuscript preparation process

During the preparation of this work the author(s) used Google Gemini in order to proofread the manuscript. After using this tool/service, the author(s) reviewed and edited the content as needed and take (s) full responsibility for the content of the published article.

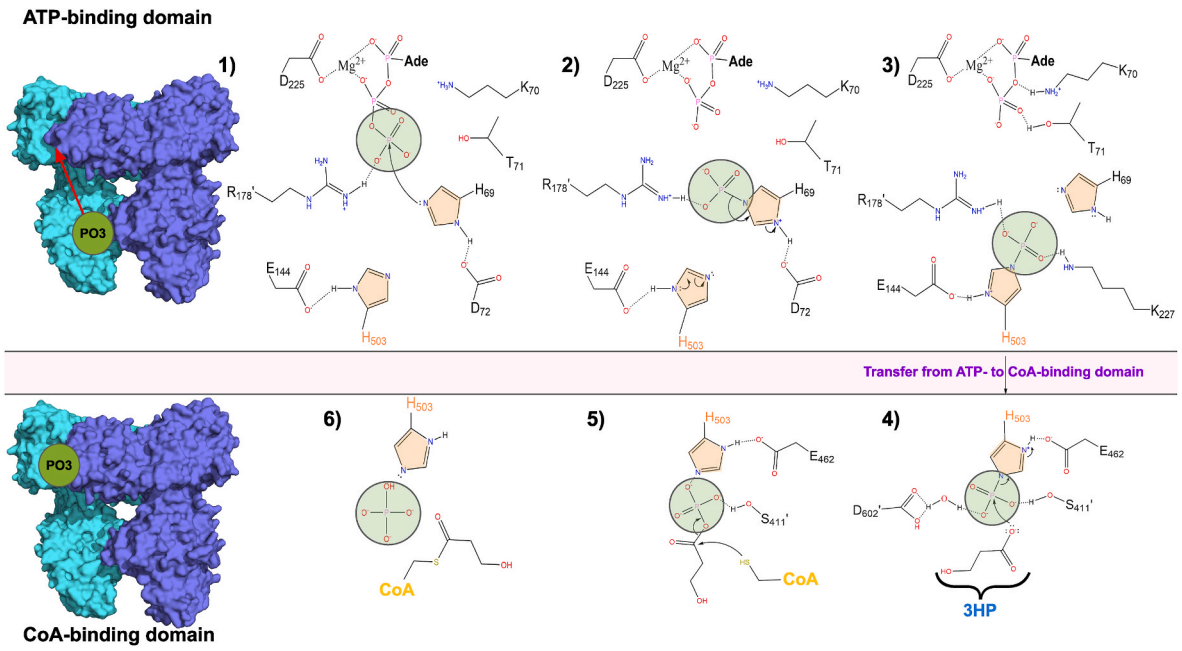

Fig. 6. Reaction mechanism of Nmar_1309

1–6 The proposed reaction mechanism of Nmar_1309 derived from homologous structures. Following ATP binding, the gamma phosphate of the ATP is dephosphorylate and passed from **1,2** H69 to **2,3** H503 on the 'swinging-loop' of subdomain 2 in the CoA-binding domain. **4,5** The 'swinging-loop' subsequently swings into the CoA-binding domain active site and is stabilized by Asp602′ and Ser411′, where it may interact with the acyl-group on 3-HP. This leads to the formation of a transient 3HP-phosphohistidine before reaction with CoA. **6** shows the products of the reaction including the free phosphate, unbound H503 and 3-hydroxypropionyl-CoA. Surface representation of the structure on the left highlights the 41Å phosphoryl transfer between domains.

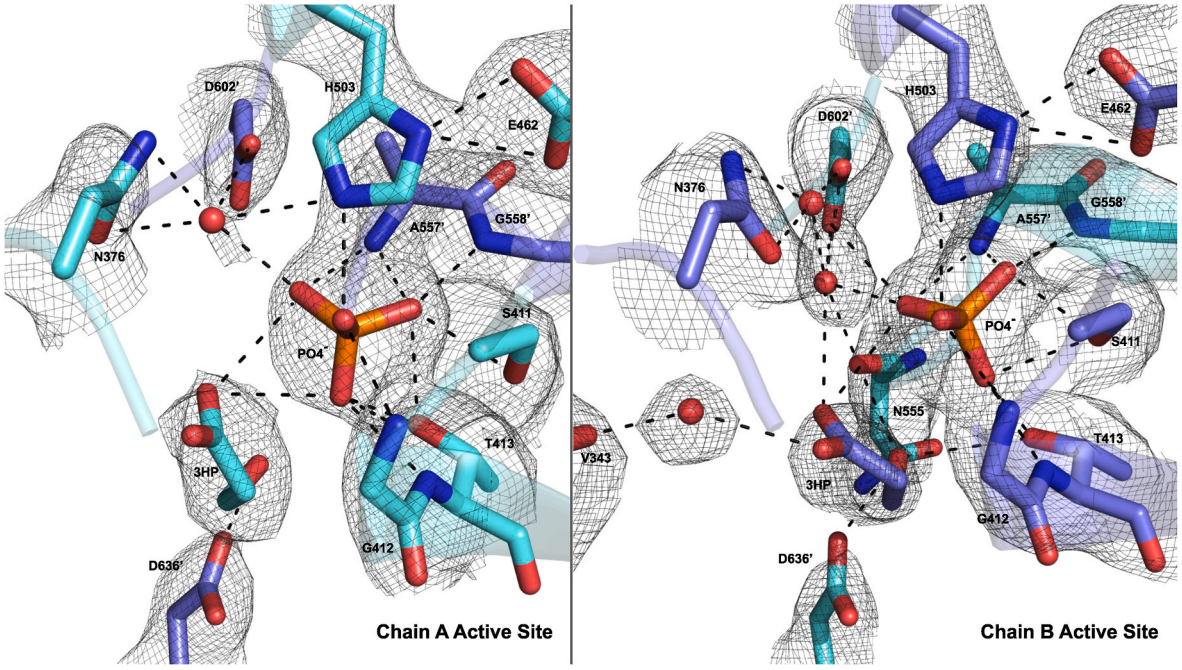

Fig. 7. Active Site interactions with bound phosphate and 3-hydroxypropionate

A free phosphate can be found at the active site bound to H503 and the ligand of interest 3-hydroxypropionate. Most interactions here are not found in the predicted reaction mechanism with the exception of those between E462 and H503; between S411 and phosphate; and between D602′, a water molecule and phosphate seen in Fig. 6 panel 4.

Funding statement

This project and the experiments are funded by TÜBİTAK-NSF 2501 bilateral research program (project number 221N355).

Declaration of competing interest

The authors declare that they have no known competing financial interests or personal relationships that could have appeared to influence the work reported in this paper.

Appendix A. Supplementary data

Supplementary data to this article can be found online at https://doi.org/10.1016/j.crstbi.2026.100189.

References

Adams, P.D., Afonine, P.V., Bunkóczi, G., Chen, V.B., Davis, I.W., Echols, N., Headd, J.J., Hung, L.-W., Kapral, G.J., Grosse-Kunstleve, R.W., McCoy, A.J., Moriarty, N.W., Oeffner, R., Read, R.J., Richardson, D.C., Richardson, J.S., Terwilliger, T.C., Zwart, P.H., 2010. PHENIX: a comprehensive Python-based system for macromolecular structure solution. Acta Crystallogr. Sect. D Biol. Crystallogr. 66 (2), 213–221. https://doi.org/10.1107/s0907444909052925.

Altschul, S.F., Gish, W., Miller, W., Myers, E.W., Lipman, D.J., 1990. Basic local alignment search tool. J. Mol. Biol. 215 (3), 403–410. https://doi.org/10.1016/S0022-2836(05)80360-2.

Altschul, S.F., Madden, T.L., Schäffer, A.A., Zhang, J., Zhang, Z., Miller, W., Lipman, D.J., 1997. Gapped BLAST and PSI-BLAST: a new generation of protein database search programs. Nucleic Acids Res. 25 (17), 3389–3402. https://doi.org/10.1093/nar/25.17.3389.

Atalay, N., Akcan, E.K., Gül, M., Ayan, E., Destan, E., Kuzucu, F.B.E., Tokay, N., Çakilkaya, B., Nergiz, Z., Usta, G.K., Kepceoğlu, A., Yapıcı, İ., Tosun, B., Baldır, N., Yıldırım, G., Johnson, J.A., Güven, Ö., Shafiei, A., Arslan, N.E., Yılmaz, M., Kulakman, C., Paydos, S.S., Çinal, S.S., Şabanoğlu, K., Pazarçeviren, A., Yılmaz, A., Canbay, B., Aşçı, B., Kartal, E., Tavlı, S., Çaliseki, M., Göç, G., Mermer, A., Yeşilay, G., Altuntaş, S., Tateishi, H., Otsuka, M., Fujita, M., Tekin, Ş., Çiftçi, H., Durdağı, S., Doğanay, G.D., Karaca, E., Türköz, B.K., Kabasakal, B.V., Katı, A., Demirci, H., 2023. Cryogenic X-ray crystallographic studies of biomacromolecules at Turkish light source "Turkish DeLight.". Turk. J. Biol. 47 (1), 1–13. https://doi.org/10.55730/1300-0152.2637.

Bailey, D.L., Fraser, M.E., Bridger, W.A., James, M.N., Wolodko, W.T., 1999. A dimeric form of *Escherichia coli* succinyl-CoA synthetase produced by site-directed mutagenesis. J. Mol. Biol. 285 (4), 1655–1666. https://doi.org/10.1006/jmbi.1998.2325.

Berg, I.A., Kockelkorn, D., Buckel, W., Fuchs, G., 2007. A 3-hydroxypropionate/4-hydroxybutyrate autotrophic carbon dioxide assimilation pathway in archaea. Science 318 (5857), 1782–1786. https://doi.org/10.1126/science.1149976.

Berman, H.M., Westbrook, J., Feng, Z., Gilliland, G., Bhat, T.N., Weissig, H., Shindyalov, I.N., Bourne, P.E., 2000. Protein data bank. Nucleic Acids Res. 28 (1), 235–242. https://doi.org/10.1093/nar/28.1.235.

Bräsen, C., Schmidt, M., Grötzinger, J., Schönheit, P., 2008. Reaction mechanism and structural model of ADP-forming Acetyl-CoA synthetase from the hyperthermophilic archaeon *Pyrococcus furiosus*: evidence for a second active site histidine residue. J. Biol. Chem. 283 (22), 15409–15418. https://doi.org/10.1074/jbc.M710218200.

DeMirci, H., Tolar, B.B., Doukov, T., Petriceks, A., Pal, A., Yoshikuni, Y., Gomez, A., Saes, D., Vöhringer-Martinez, E., Schwander, T., Erb, T.J., Francis, C.A., Wakatsuki, S., 2020. Structural adaptation of oxygen tolerance in 4-hydroxybutyrl-CoA dehydratase, a key enzyme of archaeal carbon fixation [Preprint] bioRxiv. 2020-02. https://doi.org/10.1101/2020.02.05.935528.

Destan, E., Yuksel, B., Tolar, B.B., Ayan, E., Deutsch, S., Yoshikuni, Y., Wakatsuki, S., DeMirci, H., 2021. Structural insights into bifunctional thaumarchaeal crotonyl-CoA hydratase and 3-hydroxypropionyl-CoA dehydratase from *Nitrosopumilus maritimus*. Sci. Rep. 11 (1). https://doi.org/10.1038/s41598-021-02180-8. Article 22849.

Emsley, P., Cowtan, K., 2004. Coot: model-building tools for molecular graphics. Acta Crystallogr. Sect. D Biol. Crystallogr. 60 (12), 2126–2132. https://doi.org/10.1107/s0907444904019158.

Fan, F., Williams, H.J., Boyer, J.G., Graham, T.L., Zhao, H., Lehr, R., Qi, H., Schwartz, B., Qi, H., Schwartz, B., Raushel, F.M., Meek, T.D., 2012. On the catalytic mechanism of human ATP citrate lyase. Biochemistry 51 (26), 5198–5211. https://doi.org/10.1021/bi300611s.

Fraser, M.E., James, M.N.G., Bridger, W.A., Wolodko, W.T., 1999. A detailed structural description of *Escherichia coli* succinyl-CoA synthetase. J. Mol. Biol. 285 (4), 1633–1653. https://doi.org/10.1006/jmbi.1998.2324.

Fraser, M.E., Joyce, M.A., Ryan, D.G., Wolodko, W.T., 2002. Two glutamate residues, Glu 208 alpha and Glu 197 beta, are crucial for phosphorylation and dephosphorylation of the active-site histidine residue in succinyl-CoA synthetase. Biochemistry 41 (2), 537–546. https://doi.org/10.1021/bi011518y.

Huang, J., Fraser, M.E., 2016. Structural basis for the binding of succinate to succinyl-CoA synthetase. Acta Crystallogr. Sect. D Biol. Crystallogr. 72 (8), 912–921. https://doi.org/10.1107/S2059798316010044.

Ingalls, A.E., Shah, S.R., Hansman, R.L., Aluwihare, L.I., Santos, G.M., Druffel, E.R., Pearson, A., 2006. Quantifying archaeal community autotrophy in the mesopelagic ocean using natural radiocarbon. Proc. Natl. Acad. Sci. 103 (17), 6442–6447. https://doi.org/10.1073/pnas.0510157103.

Johnson, J., Tolar, B.B., Tosun, B., Yoshikuni, Y., Francis, C.A., Wakatsuki, S., DeMirci, H., 2024. Crystal structure of the 4-hydroxybutyryl-CoA synthetase (ADP-forming) from *Nitrosopumilus maritimus*. Commun. Biol. 7 (1), 1364. https://doi.org/10.1038/s42003-024-06432-x.

Joyce, M.A., Fraser, M.E., James, M.N., Bridger, W.A., Wolodko, W.T., 2000. ADP-binding site of *Escherichia coli* succinyl-CoA synthetase revealed by x-ray crystallography. Biochemistry 39 (1), 17–25. https://doi.org/10.1021/bi991696f.

Kabsch, W., 2010. XDS. Acta Crystallogr. Sect. D Biol. Crystallogr. 66 (2), 125–132. https://doi.org/10.1107/S0907444909047337.

Könneke, M., Schubert, D.M., Brown, P.C., Hügler, M., Standfest, S., Schwander, T., Schada von Borzyskowski, L., Erb, T.J., Stahl, D.A., Berg, I.A., 2014. Ammonia-oxidizing archaea use the most energy-efficient aerobic pathway for CO2 fixation. Proc. Natl. Acad. Sci. 111 (22), 8239–8244. https://doi.org/10.1073/pnas.1402028111.

Letunic, I., Bork, P., 2021. Interactive tree of life (iTOL) v5: an online tool for phylogenetic tree display and annotation. Nucleic Acids Res. 49 (W1), W293–W296. https://doi.org/10.1093/nar/gkab301.

Levy, E.D., Teichmann, S.A., 2013. Structural, evolutionary, and assembly principles of protein oligomerization. In: Conn, P.M. (Ed.), Progress in Molecular Biology and Translational Science, 117. Academic Press, pp. 25–51. https://doi.org/10.1016/b978-0-12-386931-9.00002-7.

Negi, S.S., Schein, C.H., Oezguen, N., Power, T.D., Braun, W., 2007. InterProSurf: a web server for predicting interacting sites on protein surfaces. Bioinformatics 23 (24), 3397–3399. https://doi.org/10.1093/bioinformatics/btm474.

Oliynyk, M., Brown, M.J.B., Cortés, J., Staunton, J., Leadlay, P.F., 1996. A hybrid modular polyketide synthase obtained by domain swapping. Chem. Biol. 3 (10), 833–839. https://doi.org/10.1016/s1074-5521(96)90069-1.

Ren, M., Feng, X., Huang, Y., Wang, H., Hu, Z., Clingenpeel, S., Swan, B.K., Fonseca, M. M., Posada, D., Stepanauskas, R., Hollibaugh, J.T., Foster, P.G., Woyke, T., Luo, H., 2019. Phylogenomics suggests oxygen availability as a driving force in Thaumarchaeota evolution. ISME J. 13 (9), 2150–2161. https://doi.org/10.1038/s41396-019-0418-8.

Saier Jr., M.H., Reizer, J., 1990. Domain shuffling during evolution of the proteins of the bacterial phosphotransferase system. Res. Microbiol. 141 (9), 1033–1038. https://doi.org/10.1016/0923-2508(90)90077-4.

Sánchez, L.B., Galperin, M.Y., Müller, M., 2000. Acetyl-CoA synthetase from the amitochondriate eukaryote *Giardia lamblia* belongs to the newly recognized superfamily of acyl-CoA synthetases (nucleoside diphosphate-forming). J. Biol. Chem. 275 (8), 5794–5803. https://doi.org/10.1074/jbc.275.8.5794.

Schrödinger, L.L.C., 2021. The PyMOL molecular graphics system. Version 2.5.2 [Computer software]. https://pymol.org.

Tamura, K., Peterson, D., Peterson, N., Stecher, G., Nei, M., Kumar, S., 2011. MEGA5: molecular evolutionary genetics analysis using maximum likelihood, evolutionary distance, and maximum parsimony methods. Mol. Biol. Evol. 28 (10), 2731–2739. https://doi.org/10.1093/molbev/msr121.

Tamura, K., Stecher, G., Kumar, S., 2021. MEGA11: molecular evolutionary genetics analysis version 11. Mol. Biol. Evol. 38 (7), 3022–3027. https://doi.org/10.1093/molbev/msab120.

Tickle, I.J., Flensburg, C., Keller, P., Paciorek, W., Sharff, A., Vonrhein, C., Bricogne, G., 2016. STARANISO. Global Phasing Ltd. http://staraniso.globalphasing.org/cgi-bin/staraniso.cgi.

Verschueren, K.H., Blanchet, C., Felix, J., Dansercoer, A., De Vos, D., Bloch, Y., Van Beeumen, J., Svergun, D., Gutsche, I., Savvides, S.N., Verstraete, K., 2019. Structure of ATP citrate lyase and the origin of citrate synthase in the Krebs cycle. Nature 568 (7753), 571–575. https://doi.org/10.1038/s41586-019-1095-5.

Weiße, R.H.-J., Faust, A., Schmidt, M., Schönheit, P., Scheidig, A.J., 2016. Structure of NDP-forming Acetyl-CoA synthetase ACD1 reveals a large rearrangement for phosphoryl transfer. Proc. Natl. Acad. Sci. 113 (5), E519–E528. https://doi.org/10.1073/pnas.1518614113.

Wolodko, W.T., Fraser, M.E., James, M.N., Bridger, W.A., 1994. The crystal structure of succinyl-CoA synthetase from *Escherichia coli* at 2.5-A resolution. J. Biol. Chem. 269 (14), 10883–10890. https://doi.org/10.1016/s0021-9258(17)34141-8.

World Meteorological Organization, 2024. State of the Global Climate 2023. https://library.wmo.int/records/item/68835-state-of-the-global-climate-2023.

Yariv, B., Yariv, E., Kessel, A., Masrati, G., Chorin, A.B., Martz, E., Mayrose, I., Pupko, T., Ben-Tal, N., 2023. Using evolutionary data to make sense of macromolecules with a "face-lifted" ConSurf. Protein Sci. 32 (3), e4582. https://doi.org/10.1002/pro.4582.